Free Volume of Molten and Glassy Polystyrene and Its Nanocomposites

Utracki, Leszek

Publisher's version / Version de l'éditeur:
http://dx.doi.org/10.1002/polb.21621
Journal of Polymer Science Part B: Polymer Physics, 46, 23, pp. 2504-2518, 2008

Free Volume of Molten and Glassy Polystyrene and Its Nanocomposites

L. A. UTRACKI

National Research Council Canada, Industrial Materials Institute, 75 de Mortagne, Boucherville, Quebec, Canada, J4B 6Y4

Received 12 November 2007; revised 10 December 2007; accepted 15 January 2008
DOI: 10.1002/polb.21621
Published online in Wiley InterScience (www.interscience.wiley.com).

ABSTRACT: The Pressure-Volume-Temperature (*PVT*) dependencies of polystyrene-based clay-containing nanocomposites (CPNC) were determined in the glassy and molten state. The *PVT* data in the melt were fitted to the Simha-Somcynsky (S-S) lattice-hole equation-of-state (eos), yielding the free volume quantity, $h = h(T, P)$, and the characteristic reducing parameters, P^*, V^*, T^*. The data within the glassy region were interpreted considering that the latter parameters are valid in the whole range of independent variables, than calculating $h = h(T, P)$ from the experimental values of $V = V(T, P)$. Next, the frozen free volume fraction in the glass was computed as FF = FF(P). In the molten state the maximum reduction of free volume was observed at $w_{solid} \approx 3.6$–wt % clay, amount sufficient to adsorb all PS into solidified layer around organoclay stacks. In the vitreous state FF increased with clay content from 0.6 to 1.6—this is the first time FF > 1 has been observed. The highest value was determined for CPNC with the highest clay content, $w = 17.1$ wt %, thus well above w_{solid}. The derivative properties, compressibility, κ, and the thermal expansion coefficient, α, depend on T, P, and w. Plots of κ versus T indicate the presence of two secondary transitions, one at $T_\beta/T_g \approx 0.9 \pm 0.1$ and other at $T_T/T_g = 1.2 \pm 0.1$. ©2008 Wiley Periodicals, Inc. J Polym Sci Part B: Polym Phys 46: 2504–2518, 2008

Keywords: equation-of-state; free volume; glass transition; nanotechnology; noncrystalline polymers; statistical thermodynamics; thermal properties; vitreous state behavior

INTRODUCTION

Polymeric Nanocomposites

Polymer nanocomposites (PNC) are composed of a polymeric matrix and dispersed in it nanoparticles, that is, platelets, fibers, or spheroids with at least one dimension of ≤ 2 nm.[1,2] PNC with all three types of nanoparticles have been prepared (e.g., polycarbonate with carbon nanotubes, polyamide with iron oxide spheres), but only PNC with clay platelets (clay-containing PNC, or CPNC) are commercially available for high-volume structural applications.

The CPNC applications range from the transport industry, to packaging, sports equipment, and so forth. For example, Ube and Unitika have been producing polyamide (PA)-based CPNC for automotive applications; Toyota develops polylactic acid (PLA)-based CPNC as replacement for polypropylene (PP); BASF developed scratch-resistant paints; GM has been using PP-based CPNC for steps, body side moldings and load floors; similarly Acura uses CPNC for seat backs and interior consoles; multilayered bottles have been produced by Bayer or Honeywell; films with enhanced barrier properties from Clariant, Honeywell, or Dow; while Wilson Sports intro-

Correspondence to: L. A. Utracki (E-mail: leszek.utracki@cnrc-nrc.gc.ca)

Journal of Polymer Science: Part B: Polymer Physics, Vol. 46, 2504–2518 (2008)

duced long-life tennis and other sport balls with reduced gas permeability. Incorporation of lamellar particles not only is responsible for enhancement of mechanical, barrier, or scratch resistant properties, but also for reduction of flammability, for controlled release of additives such as biocides and dyes, as well as for catalytic activities. The global market share of CPNC is expected to reach about US$ 4 billion by 2008. Nevertheless, several technological problems still remain, and behavior of these systems is often difficult to control.

The main aspect of CPNC that controls its behavior is the degree of platelets dispersion. The nomenclature proposed by IUPAC recommends that the term "nano" is used only when at least one dimension of a particle is $\leq$2 nm, meso- when it ranges from 2 to 50 nm, and micro- above 50 nm. Thus, material with platelets assembled in stacks or aggregates should not be called nanocomposites. However, since in this work a range of compositions was examined, to avoid confusing change of nomenclature the abbreviation "CPNC" will be used for all systems.

The degree of clay dispersion is controlled by two factors—first, by the thermodynamic miscibility between clay, intercalant, and polymer, second by the clay concentration. It can be shown that the fully exfoliated CPNC must contain not more than 1.14 wt % of inorganic clay, having an aspect ratio of about 280, as in most commercial organoclays. Above this limit, as the concentration increases the stacks are formed with decreasing interlayer spacings. Different CPNC properties show best performance at different concentrations, for example, for the mechanical performance the optimum is at nanodispersion, while for the barrier performance it falls within the mesodispersion range.

Pressure-Volume-Temperature Measurements

The pressure-volume-temperature (*PVT*) measurements of CPNC are relatively scarce, performed in few laboratories around the world. Even for the determination of compressibility, κ, and the thermal expansion coefficients α:

$$\kappa \equiv -\left(\frac{\partial \ln V}{\partial P}\right)_{T,P^0,q}; \quad \alpha \equiv \left(\frac{\partial \ln V}{\partial T}\right)_{T^0,P,q} \tag{1}$$

simpler, single value methods are used (viz. ASTM D696, ISO 11,359, JIS K7197). In eq 1 P^0 and T^0 are the glass forming pressure and temperature, respectively, and q is the rate of heating or compressing.

However, there is much more information accessible from *PVT* data than κ and α. By comparing the experimental information with theoretical predictions one might determine free volume as functions of independent variables (e.g., *P*, *T*, composition), as well as the Lennard-Jones (L-J) intermolecular attraction and repulsion parameters. Furthermore, for the binary systems such as CPNC the *PVT* data yields information about interactions between the two constituents. Such analyses of molten CPNC have been published.[3–5]

A number of equations of state (eos) have been proposed for molten polymer.[6] By contrast, rigorous analyses of the *PVT* behavior in the vitreous state are rare, as the thermodynamic history and time-dependent glass structures complicate the experiments and their interpretation. The preceding publications have been limited either to molten CPNC or to glassy amorphous polymers. The present one attempts to analyze the effects of organoclay addition on CPNC properties within the full range of *P* and *T*.

THEORY

Molten State

The Simha-Somcynsky (S-S) lattice-hole theory was derived for spherical and chain molecule fluids.[7,8] The model lattice contains volume fraction y of occupied sites and, $h = 1-y$, of unoccupied sites (or holes). For liquids under the thermodynamic equilibrium conditions, from the Helmholtz free energy, *F*, the S-S eos was obtained:[7]

$$\tilde{P}\tilde{V}/\tilde{T} = (1-U)^{-1} + 2yQ^2(AQ^2 - B)/\tilde{T} \tag{2}$$

$$3c\left[(U-1/3)/(1-U) - yQ^2(3AQ^2 - 2B)/6\tilde{T}\right] + (1-s) - (s/y)\ln(1-y) = 0 \tag{3}$$

where $Q = 1/(y\tilde{V})$, $U = 2^{-1/6}\ yQ^{1/3}$, $A = 1.011$ and $B = 1.2045$ (for the face-centered cubic lattice). Equation 2 was derived from the thermodynamic definition of pressure, $\tilde{P} = -(\partial\tilde{F}/\partial\tilde{V})_{\tilde{T}}$, while eq 3 from the minimization of free energy as function of the free volume content, $(\partial\tilde{F}/\partial h)_{\tilde{T},\tilde{V}} = 0$, thus it is only valid in liquids at

the thermodynamic equilibrium, not in the vitreous state. The variables marked by tilde are reduced:

$$\left.\begin{aligned} &\tilde{P} = P/P^*; \quad P^* = zq\varepsilon^*/(sv^*) \\ &\tilde{T} = T/T^*; \quad T^* = zq\varepsilon^*/(Rc) \\ &\tilde{V} = V/V^*; \quad V^* = v^*/M_s \end{aligned}\right\} (P^*V^*/T^*)M_s = Rc/s \tag{4}$$

The characteristic parameters, P^*, T^*, V^*, contain the L-J interaction parameters: the maximum attractive energy, ε^*, and the segmental repulsion volume, v^*, per statistical segment. The latter is defined as $M_s = M_n/s$, where M_n is the number-average molecular weight and s is the number of statistical segments. The parameter $3c$ indicates the external, volume-dependent degrees of freedom; $R = 8.3145$ [kPa L/(K mol)] is the gas constant; and $zq = s(z-2) + 2$ is the number of interchain contacts in a lattice of the coordination number $z = 12$.

Equations 2–4 describe the *PVT* liquid surface, and associated with it the free volume quantity, $h = h(\tilde{V}, \tilde{T})$. Through T^* and V^* the *PVT* data yield the L-J measures, ε^* and v^*. Since for linear molecules the flexibility index, $3c/s = 1 + 3/s$,[9] for high-molecular weight polymers, $\lim_{s\to\infty}(3c/s) = 1$. Thus, from eq 4 the L-J parameters are given by simple proportionalities:

$$\varepsilon^* \approx RT^*/30 = 2.771T^* \text{ and } v^* = V^*M_s.$$

Jain and Simha extended the original S-S theory to binary mixtures. The scaled eqs 2 and 3 were found to retain validity, but with the interaction parameters ε^* and v^* replaced by compositional averages:[10,11]

$$\langle\varepsilon^*\rangle\langle v^*\rangle^p = X_1^2\varepsilon_{11}^* v_{11}^{*p} + 2X_1X_2\varepsilon_{12}^* v_{12}^{*p} + X_2^2\varepsilon_{22}^{*p}; \quad p \in [2,4] \tag{5}$$

with the site fractions X_1 and $X_2 = 1-X_1$ defined in terms of the mole fractions $x_1 = 1-x_2$, as:

$$X_1 = q_1zX_1/(q_1zX_1 + q_2zX_2) \tag{6}$$

However, since CPNC usually contains a polymer, inorganic nano-filler particles, intercalant(s), and compatibilizer(s) the system needs to be redefined as a matrix (index #1) and dispersed solid particles (index #2).[12,13] This might be done accepting the "hairy clay particles" (HCP) model of CPNC.[14] Theory[15] and experiments[16–18] revealed that in the orthogonal direction from the clay platelet surface, z, there is a solidified organic layer $z_1 \approx 4$–6 nm thick, followed up by a second layer ($z_2 \approx 100$–120 nm) where the molecular mobility progressively increases with z. As a consequence, CPNC matrix is the liquid phase at a distance from the clay surface, $z > z_1$ with the interaction parameters, ε_{11}^* and v_{11}^*, while the clay platelets with $z_1 \approx 4$–6 nm thick layer of solidified organics form the dispersed phase (interaction parameters, ε_{22}^* and v_{22}^*). To describe variation of the interaction parameters with distance from the clay surface, an exponential function was adopted:[5]

$$y(z) \times \frac{y_1y_2}{y_1 - (y_1 - y_2)\exp\{n[(z-z_1)/(z-z_2)]\}}; \quad z_1 \le z < z_2; \quad y \in [\varepsilon^*, v^*] \tag{7}$$

where n is a disposable parameter (usually $n = 2$), y_1 and y_2 are the L-J parameters at the solidified polymer at z_1 and z_2, respectively. The amount of molten polymer with bulk properties decreases with the clay content; vanishing at clay content of ~0.4 vol % (the secondary layer with reduced mobility vanishes at about 7 vol %).

Glass and Other Transitions

The glass transition temperature (T_g) is kinetic in nature, thus it depends on the cooling or compressing rate, q, on P during cooling or T during compressing, and so forth.[19–22] The pressure dependence of T_g was derived by Quach and Simha as:[23,24]

$$dT_g/dP = (\partial T/\partial h)_h + (\partial T/\partial h)_P(dh_g/dP) \cong \Delta\kappa/\Delta\alpha + (\partial T/\partial h)_P(dh_g/dP) \tag{8}$$

where $(\partial T/\partial h)_P$ is computed from the isobaric data in the molten state near T_g, and $dh_g/dP = dh(T_g, P_g)/dP$. Equation 8 reduces to the Ehrenfest relation when $dh_g/dP = 0$, that is, postulating that liquid disorder near T_g is independent of pressure.

For amorphous polymers T_g is the main, but not the only transition. In addition, at $T < T_g$ there are several transitions, of which the β-one, $T_\beta \approx 0.8 \times T_g$, is nearest to T_g. The β-transition is important since the rate of physical aging is zero at T_β and T_g, reaching maximum about half way between these two, that is, $T_{max} \approx 0.88 \times T_g$.[25] At $T > T_g$ several relaxation processes

take place leading to a transition at $T_T/T_g \approx 1.2 \pm 0.1$.[6] Within this temperature range Boyer postulated existence of a "liquid–liquid" transition, T_{LL}.[19–21] More recent mechanisms deduced by molecular modeling and/or NMR measurements postulate that the crossover transition temperature, $T_c/T_g \approx 1.25 \pm 0.1$, originates from different mechanism of structural and segmental relaxations (the mode-coupling theory, MCT).[26,27] Ngai extended the MCT to the cooperative relaxation systems observed in molten polymers.[28,29]

The Vitreous State

For the vitreous state eqs 2 and 3 are not valid; in the absence of the thermodynamic equilibrium the pressure is given as:[30–32]

$$-\tilde{P} = (\partial \tilde{F}/\partial \tilde{V})_{\tilde{T},y} + (\partial \tilde{F}/\partial y)_{\tilde{V},\tilde{T}}(\partial y/\partial \tilde{V})_{\tilde{T}} \quad (9)$$

reducing at equilibrium to the standard definition of P (used for deriving eq 2). McKinney and Simha compared the results of computations using eq 2 (the so called "simplified" procedure) or eq 9. They found that the functional trends were the same and that the numerical differences were comparable to the experimental errors. Thus, as before, the simplified procedure will be used for analysis of the present data.[6,23,30–33]

The vitreous state behavior will be analyzed in four steps: (1) Calculation of the P^*, T^*, V^* parameters from the PVT data at $T > T_g$; (2) Calculation from eqs 2 and 3 the fictitious hole fractions at $T' < T_g$ and $P' < P_g$ as $h_{extrapol} = h(T', P')$; (3) Following the simplified procedure, calculation from eq 2 the hole fraction in the vitreous state: $h_{glass} = h(T', P')$; and (4) Using the isobaric values calculation of the frozen fraction:[23,24]

$$FF = 1 - (\partial h/\partial T')_{P,glass}/(\partial h/\partial T')_{P,extrapol} \quad (10)$$

The parameter FF is a fraction of the free volume trapped by vitrified segments; mainly the nonfrozen fraction, 1−FF, contributes to the material behavior in glass.

PVT MEASUREMENTS

The PS-based CPNC samples are listed in Table 1. These were prepared by melt compounding PS with organoclay in a twin screw extruder equipped with a high stress screws at $T = 200$ °C, and throughput $Q = 5$ kg/h. The matrix was commercial PS-1301 from Nova Chemicals with weight-average molecular weight $M_w = 270$ kg/mol, melt flow rate MFR = 3.5 g/10 min, and density $\rho = 1.04$ g/mL. The organoclay, Cloisite® 10A (C10A) from Southern Clay Products, is Wyoming montmorillonite (MMT) preintercalated with 39 wt % of dimethyl-benzyl hydrogenated tallow ammonium chloride (2MBHTA). The ingredients characteristics, compounding procedure, and influence of processing conditions on clay dispersion and properties have been published.[34–36]

Table 1. CPNC Studied in This Work[34–36]

No.	CPNC[a]	MMT (wt %)	V (mL/g)[b]	d_{001} (nm)[c]	m[d]
0	C10A	61	–	1.93	–
1	PS	0	0.93710	–	–
2	CPNC-1	1.4	0.93251	4.9	3.3
3	CPNC-2	2.8	0.92793	–	–
4	CPNC-5	5.7	0.91843	4.02	3.7
5	CPNC-10	10.6	0.90237	4.18	3.3
6	CPNC-17	17.1	0.88108	–	–

[a] Sample code used in the text.
[b] Specific volume at $T = 516.84$ K and $P = 190$ MPa.
[c] Interlayer spacing from first XRD peak.
[d] Number of clay platelets in stack (peak #1).

Prior to PVT measurements, the sample pellets were dried, and the specific volume under ambient conditions was determined by the immersion method.[37] Dry pellets were loaded into Gnomix pressure dilatometer (from Gnomix, Boulder, CO), pressurized to 10 MPa, premolded at $T \geq 130$ °C for 10 min, and then cooled to ~30 °C at a rate of 2.5 °C/min. The void-free specimens were tested following the "standard" procedure, that is, starting at the lowest T and P isothermally increasing pressure in steps, then reduce P, heat the specimen to higher temperature, and so forth. Thus, P increased from about 10 to 190 MPa in steps of 20 or 30 MPa and T from about 30 to 250 °C in steps of 10 °C (small effects of adiabatic heating were observed). The advantage of this procedure is that specimens see the high temperature only at the end of the test, thus they are not affected by the thermal degradation.

To confirm data accuracy the tests were repeated 2–5 times using different holding times between measurements. The total run time was 18–32 h. The average error for the specific vol-

ume (V) was $\leq 0.03\%$. The *PVT* plots in Figures 1 and 2 show the dependencies for the PS matrix and CPNC with the highest clay content. The range of the independent variables usually extended from below T_β to above T_T (for PS-1301 at $P = 0.1$ MPa the secondary transitions are at $T_\beta \cong 290-310$ K, and $T_T \cong 420-440$ K), but they are not detectable on the *PVT* surface.[38]

The *PVT* data are plotted as isobars of ln V versus $T^{3/2}$ or V versus T. The former shows wider range of linearity than the latter and it has been used by Simha et al., for example, for linearization of the V–T data and extraction of the V^* and T^* reducing parameters at $P = 0$.[38,39] The straight lines in Figure 1 are fitted to data within the glassy and molten region. Furthermore, in the Figure 1 two T_g definitions are presented: T_{g1} represent the boundary temperature between the melt and transition region, **T**,[3–6] whereas T_{g2} is the temperature at which the lines fitted to V–T data in the molten and glassy regions intersect.[40–42] At ambient pressure the two methods are in good agreement, but as P and w increase T_{g2} becomes inconsistent with the differential scanning calorimeter (DSC; see column 6 of Table 3). Thus, in the following text $T_g = T_{g1} = T_g$ (DSC) will be used.

In Figure 1, the transition zone **T** is limited by two straight lines: $T_g(0) = T_g(P = 0)$, and

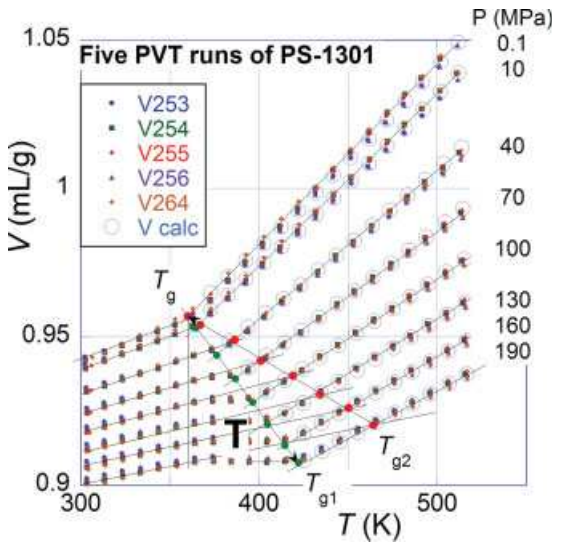

Figure 1. Results of five *PVT* runs for PS-1301 at $T = 373$–517 K and $P = 0.1$–190 MPa. The black straight lines are fitted to data within the glassy and molten region, the red ones to data within the transient region.

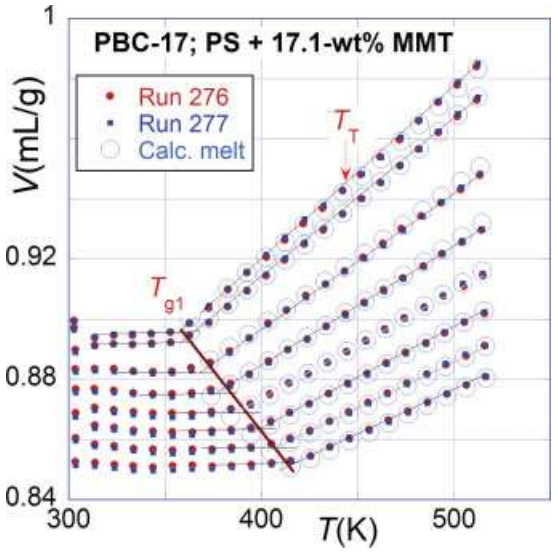

Figure 2. Results of two *PVT* runs for CPNC-17 at $T = 303$–517 K, and $P = 1$–190 MPa. The straight lines are fitted to data within the transient and molten region. Transition temperatures, $T_{g1} = T_g$ and T_T are indicated; see text.

$T_g = T_{g1}$. Here, the volume expands with increasing temperature in the vitreous and the molten state. The behavior of CPNC-17 in Figure 2 is different. The transition region is ill-defined and at $T < T_g$ the specific volume, V, initially decreases with increasing T, then becomes independent of it, and finally in the vicinity of T_g it starts increasing toward the regular melt behavior. Thus, addition of clay affects the glass volume behavior at $300 < T$ (K) $< T_g$; as the clay content increases the thermal expansion coefficient of glassy CPNC progressively decreases reaching negative values—CPNC glass shrinks upon heating from below T_β (K) $= T_{\beta 0} + 0.21P$ (MPa).[25,42]

CALCULATIONS OF THE *PVT* DEPENDENCIES USING S-S eos

Analysis of the *PVT* behavior progresses from the molten state, through the glass transition region to the vitreous state:

1. From *PVT* data of the melts calculate P^*, T^*, V^*, and the free volume, $h = h(V, T)$.
2. Determine $T_g = T_g(P, w)$, and the corresponding hole fractions at T_g, $h_g = h_g(P, w)$.

Table 2. The Characteristic Reducing Parameters and the Statistical Fit Data

CPNC	C10A (wt %)	P^* (bar)	T^* (K)	$10^4 \times V^*$ (mL/g)	M_s (g/mol)	$\langle\varepsilon^*\rangle$	$\langle v^*\rangle$	σ	r^2	CD
PS-1301	0	7432 ± 25	11542 ± 21	9311 ± 5	46.22	31.98	43.04	0.00112	0.999999	0.998847
CPNC-1	1.4	7515 ± 34	11936 ± 30	9306 ± 6	47.30	33.07	44.02	0.00096	0.999999	0.999098
CPNC-2	2.8	7475 ± 32	12014 ± 29	9274 ± 6	48.02	33.29	44.53	0.00089	0.999999	0.999206
CPNC-5	5.7	7522 ± 35	12014 ± 30	9175 ± 6	48.24	33.29	44.26	0.00088	0.999999	0.999235
CPNC-10	10.6	7470 ± 43	11847 ± 37	8990 ± 7	48.89	32.83	43.95	0.00117	0.999998	0.999306
CPNC-17	17.1	7503 ± 33	11720 ± 28	8765 ± 5	49.39	32.48	43.29	0.00094	0.999999	0.999075

3. Calculate the hole fraction in the glass, $h = h(P', T')$, and then the pressure and composition dependencies of the frozen free volume fraction, $FF_T = FF(P, w)$.

PVT Behavior in Molten State

The *PVT* data at $T > T_g$ from all runs were combined (~500 data sets) and simultaneously fitted to S-S eos following the two-step procedure.[3–6] Table 2 lists the computed P^*, T^*, V^* parameters, calculated from these M_s, $\langle\varepsilon^*\rangle$, $\langle v^*\rangle$, along with the goodness of fit measures for V: σ = standard deviation, r^2 = correlation coefficient squared, and CD = coefficient of determination; evidently S-S eos equally well describes CPNC and PS data.

The T-dependence of the free volume parameter, h, for three compositions at three P-levels is illustrated in Figure 3. The data indicate that at all levels of P the highest h-value is observed for PS, and the lowest for CPNC-2. Consequently, in Figure 4 the relative loss of free volume: $\Delta h \equiv (h_{PS} - h_{CPNC})/h_{PS}$, at ambient P and three temperatures is plotted versus clay content. The curve-fit to data indicates that the maximum loss of free volume occurs at $w_{solid} \approx 3.6$ wt % MMT loading.

The Glass Transition Temperature

The pressure dependence of glass transition temperature (T_g) was calculated from the isobaric plots of ln V versus $T^{3/2}$ (see Figs. 1 and 2). The data are well described by the second order polynomial; values of its a_i parameters are listed in Table 3. These depend on clay content as: $a_1 = 0.480 - 0.0118w$ ($r = 0.79$) and $a_2 \times 10^4 = -7.31 + 0.406\ w$ ($r = 0.77$). At $P \to 0$ the first

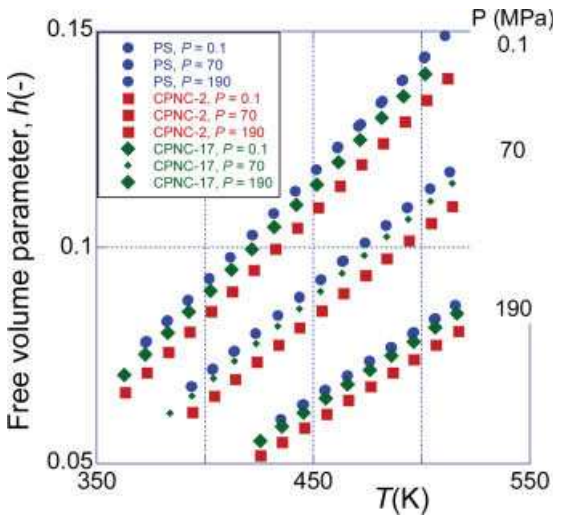

Figure 3. T-dependence of the free volume parameter, h, for PS, CPNC-2, and CPNC-17 at $P = 0.1$, 70, and 190 MPa. Note the nonlinear clay content effect. [Color figure can be viewed in the online issue, which is available at www.interscience.wiley.com.]

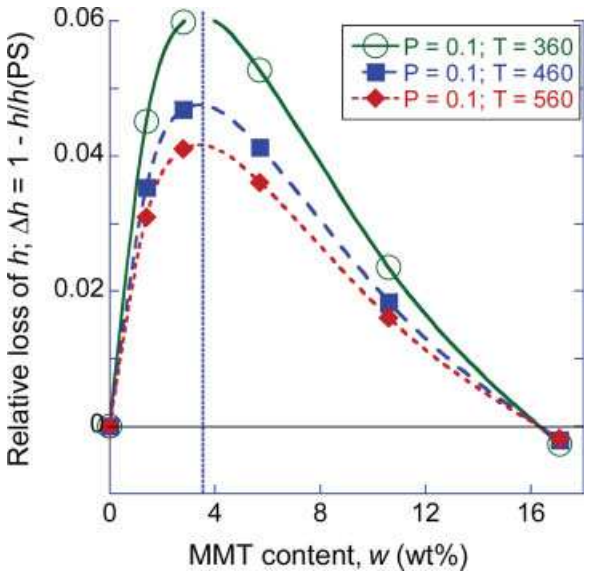

Figure 4. Relative loss of free volume for the PS-based CPNC at ambient pressure, $P = 0.1$ MPa, and indicated temperatures, T(K). [Color figure can be viewed in the online issue, which is available at www.interscience.wiley.com.]

Table 3. Pressure Dependence of the Glass Transition Temperature: $T_g = \Sigma a_i P^i$; and the Hole Fraction at T_g: $h_g = h_{g0} + b_1 P$ (MPa)

Sample	$T_{g,P=0}$	a_1	$a_2 \times 10^4$	r	$T_{g,P=0}$(DSC)	h_{g0}	$-b_1 \times 10^4$	r
PS	357.6	0.491	−8.14	0.998	365.4	0.0682	7.40	0.991
CPNC-1	360.4	0.430	−4.78	0.998	364.9	0.0650	7.16	0.994
CPNC-2	349.9	0.531	−8.65	0.989	363.4	0.0608	5.36	0.915
CPNC-5	361.0	0.271	−2.12	0.998	362.0	0.0639	8.00	0.969
CPNC-10	353.0	0.383	−5.11	0.999	360.9	0.0637	8.44	0.997
CPNC-17	356.7	0.338	0.09	1.000	357.1	0.0638	8.60	0.981

derivative decreases with w from $(dT_g/dP)_{P=0} = 0.480$ to 0.278 (K/MPa), while the second derivative increases from -1.46×10^{-3} to -7.35×10^{-5}.

The computed hole fraction, $h_g = h_g(T_g, P)$, linearly decreases with P (see Table 3). In contrast with T_g and its derivatives, the h_g varies nonlinearly with clay content. The data suggest that at $w_{solid} \approx 3.6$ wt % MMT CPNC is most sensitive to P.

Vitreous Region at $T' < T_g$

It is convenient to distinguish the independent variables in the glassy state by primes, viz. T', P' and calculate the hole fraction within the glassy region, $h_{glass} = h(T', P')$, from the PVT data, by substituting $V = V(T', P')$ into eq 2, for which the P^*, T^*, V^* parameters are already known.[6,24] Next, the hole fraction that melt would have if existed at T' and P', $h_{extrapol} = h(T', P')$, is computed from eqs 2 and 3. For clay content >5 wt % the free volume, h_{glass}, decreases with T; most rapidly at $304 < T(K) < 314$, that is, in the vicinity of T_β at $T/T_g \approx 0.86 \pm 0.02$.

The free volume frozen fraction, FF (see Table 4), was calculated from eq 10 using computed values of $(\partial h/\partial T')_{P,glass}$ and $(\partial h/\partial T')_{P,extrapol}$. The isobaric clay-content dependence is nonmonotonic, with local minimum at MMT content of $w_{solid} = 3.6$ wt %. It is noteworthy that while for neat polymers FF < 0.9, for CPNC, FF > 1; these high values are unprecedented.

COMPRESSIBILITY AND THERMAL EXPANSION COEFFICIENTS

The defined in eq 1 compressibility, κ, and thermal expansion, α, coefficients were calculated from raw data plotted as ln V versus P or T using the moving arch computational methods. An example of the κ versus T plots are presented in Figure 5 (the initial data points at $T < 320$ K were omitted), and that of α versus T in Figure 6. The glass transition and the upper transition at $T_T/T_g \approx 1.2 \pm 0.1$ are readily visible. Addition of clay reduces the κ versus T dependence in the glass toward negative values. Note that in Figure 5 T_g and T_T seems independent of P—the pressure dependence of T_g from ln V versus $T^{3/2}$ is marked by solid line with negative slope dividing the large transition region, **T**.

DISCUSSION

Molten State: L-J Interactions and Free Volume

The data in Table 2 confirm that within the full range of clay content, $w = 0$–17.1 wt %, S-S eos

Table 4. Free Volume Frozen Fraction (FF) of PS and Its PNC's

P (MPa)	PS	CPNC-1	CPNC-2	CPNC5	CPNC-10	CPNC-17
0.1	0.62994	0.75220	0.73348	0.9582	1.0507	1.1798
10	0.65665	0.77350	0.75455	0.9927	1.1150	1.2389
40	0.73364	0.83976	0.81262	1.0872	1.2934	1.4030
70	0.75884	0.87018	0.83566	1.1503	1.3686	1.4900
100	0.78189	0.88023	0.85029	1.1877	1.4454	1.5852
130	0.79624	0.91088	0.85015	1.2454	1.4929	1.6513
160	0.84049	0.92701	0.88066	1.2776	1.5044	1.6748
190	0.85584	0.96829	0.88850	1.3028	1.4579	1.5807

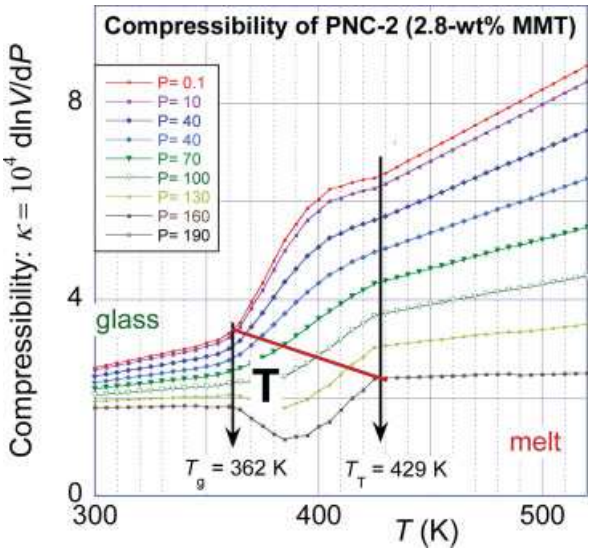

Figure 5. Volume compressibility versus T for PNC-2. Red inclined line indicates T_{g1}. [Color figure can be viewed in the online issue, which is available at www.interscience.wiley.com.]

well describes the *PVT* surface. The calculated from P^*, T^*, V^* volume-averaged Lennard-Jones interaction parameters, $\langle\varepsilon^*\rangle$ and $\langle v^*\rangle$, are shown in columns 7 and 8; both parameters plotted versus MMT content go through a maximum at $w \approx 3.6$ wt % MMT. Linearity found for neat PS: $\varepsilon^* = 13.4 + 0.445v^*$ ($r = 0.952$),[43] is also observed for the bulk-average parameters of CPNC: $\langle\varepsilon^*\rangle = -5.23 + 0.868\ \langle v^*\rangle$ ($r = 0.968$). However, in CPNC the relation between ε^* and v^* is stronger, with the slope nearly twice as large as that for neat PS.

The next task is determination of the six individual binary interaction parameters from the bulk-average components using eqs 5–7. First, the molar and site fractions (x_i, and X_i, respectively) are calculated. The molar fraction of the polymer, x_1, is reduced by solidification on the clay:

$$x_1 = \frac{(m_1/M_{s1}) - (m_{1,\mathrm{Solid}}/M_{s1})}{(m_1/M_{s1}) + (m_2/M_{s2})} \qquad (11)$$

where m_1 is the weight fraction of the polymer, $m_{1,\mathrm{Solid}}$ is its solidified weight fraction, m_2 is clay weight fraction, and $M_{si} = M_i/s_i$ is the molecular weight of statistical segment of component "i" (M_i and s_i are molecular weight and number of statistical segments, respectively). The segmental MW of PS in Table 2 is $M_{s1} = 46.22$ (g/mol), whereas the molecular weight of styrene is $M_0 = 104.14$ g/mol, thus one lattice cell accommodates about ½ of styrene mer with the hard core molecular volume of $v^*_{\mathrm{hard}} = 43.035/2^{1/2} = 30.43$ (mL/mol). The hard-core statistical segment of clay should occupy a similar lattice volume. This rule provides means for computing the molecular weight of the clay statistical segment, M_{s2}. The clay platelets are assumed to be circular with average diameter of $d = 200$ nm, thickness $h = 0.96$ nm, and density $\sigma = 2.3$ g/mL; hence the "molecular mass" of an average platelet is: $M_2 = N_A\rho\pi d^2 h/4 = 41{,}772$ (kg/mol), and its volume is: $V_{\mathrm{plat}} = M/\rho = 4.54 \times 10^6$ (mL/mol). In consequence, the number of segments for PS (s_1) and clay (s_2) are respectively: $s_1 = 2921$ and $s_2 = V_{\mathrm{plat}}/v^*_{\mathrm{hard}} = 3.43 \times 10^5$.

Next, the mass of solidified PS on the surface of clay platelet is calculated. For fully exfoliated clay platelets this has been done based on the relative volume of solidified, 6 nm thick layer of polymer adsorbed onto clay surface, A.[4] However, the melt compounded PS/C10A systems are only intercalated. The first XRD peak-1 indicates progressive reduction of the interlayer spacing ($d_{001} \approx 4.9$–4.0 nm) and intensity with clay content.[34–36] Furthermore, the HRTEM micrographs shows that the CPNC morphology is dominated by tightly packed stacks corresponding to peak-2 ($d_{001} \approx 1.4$ nm) with about 6 platelets each. The dimensions and spacing within the stacks was independent of concentra-

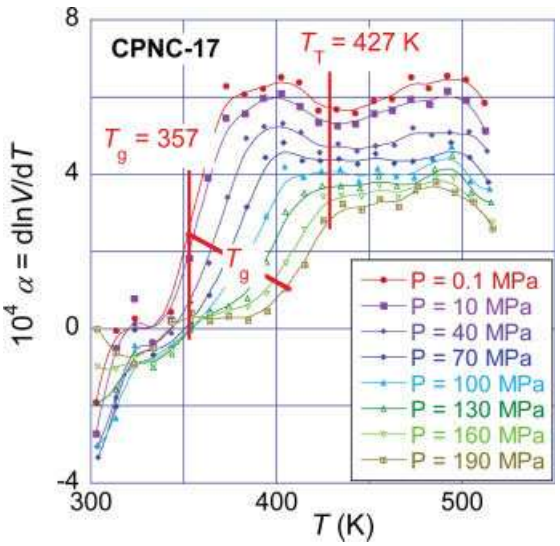

Figure 6. Thermal expansion coefficient versus T for PNC-10. Red inclined line indicates T_{g1}. [Color figure can be viewed in the online issue, which is available at www.interscience.wiley.com.]

tion, behaving as effective particles composed of intercalated clay platelets. From the stacks geometry the intercalant content was calculated as about 24 wt %, instead of 39 wt % as in organoclay, what might indicate dissolution in PS matrix of the excess intercalant (above the clay cation exchange capacity, CEC) and/or a partial degradation during compounding. Consequently, the CPNC might be visualized as PS matrix and dispersed in it stacks having effective diameter $\geq$200 nm and thickness, $h_{\text{eff}} \approx 11$ nm. However, since the platelets are rarely stacked in uniform box-like forms their effective aspect ratio, p_{eff}, might be significantly larger and in consequence the volume fraction of encompassed particles, $\phi_{\max}$, may range from 1.4 wt % (full exfoliation) to 10.7 wt % (stacks with $p_{\text{eff}} \geq 18$).

The PS solidification on the observed stacks assuming 4 nm thick solidified organic indicates that the limiting concentration for nonsolidified PS is $w_{\text{solid}} = 3.6$ wt %. As evident in Figure 4, relative loss of the matrix free volume quantity, Δh, reaches maximum at this very concentration. Similarly, the maximum values of the L-J bulk-average interaction parameters, pressure sensitivity of T_g, and other measures of the material behavior show extrema near w_{solid}.

Of the six L-J parameters in eqs 5–7 two (ε_{11}^* and v_{11}^*) are experimentally accessible, while, as before,[5] the cross-interaction parameters, ε_{12}^* and v_{12}^*, might be taken as geometric and algebraic averages, respectively:

$$\varepsilon_{12}^* = \sqrt{\varepsilon_{11}^* \varepsilon_{22}^*}\ ; \text{ and } v_{12}^* = \left[v_{11}^{*1/3} + v_{22}^{*1/3}\right]^3/8 \quad (12)$$

For computational convenience eq 5 was transformed into:[1]

$$\langle v^* \rangle^2 = \frac{\Xi_4}{\Xi_2} \times v_{11}^{*2};\ \text{and}\ \langle \varepsilon^* \rangle = \frac{\Xi_2^2}{\Xi_4} \times \varepsilon_{11}^*$$
$$\Xi_2 \equiv X_1^2 + 2X_1X_2e_{12}v_{12}^2 + X_2^2e_{22}v_{22}^2 = \left(\frac{\langle v^* \rangle}{v_{11}^*}\right)^2 \left(\frac{\langle \varepsilon^* \rangle}{\varepsilon_{11}^*}\right) \quad (13)$$
$$\Xi_4 \equiv X_1^2 + 2X_1X_2e_{12}v_{12}^4 + X_2^2e_{22}v_{22}^4 = \left(\frac{\langle v^* \rangle}{v_{11}^*}\right)^4 \left(\frac{\langle \varepsilon^* \rangle}{\varepsilon_{11}^*}\right)$$

with the following definitions:

$$e_{12} \equiv \varepsilon_{12}^*/\varepsilon_{11}^*; \quad e_{22} \equiv \varepsilon_{22}^*/\varepsilon_{11}^*;$$
$$v_{12} \equiv v_{12}^*/v_{11}^*; \quad v_{22} \equiv v_{22}^*/v_{11}^*.$$

Optimized fit (with $r^2 = 0.99997$) of the bulk-averaged interaction parameters to eqs 12 and 13 was achieved using Scientist program from MicroMath. The results are listed in Table 5. It is noteworthy that the ratio: $v_{22}^*/v_{11}^* = 1.03$, hence it is within the theoretically acceptable range for the lattice cell size variation.[13]

Table 5. Binary Interaction Parameters for PS/MMT Stacks System at $\phi > \phi_{\max}$

	Binary Interactions		
Parameters	ij = 11	12	22
ε_{ij}^*	32.0 ± 0.6	32.5 ± 0.4	33.0 ± 0.1
v_{ij}^*	43.0 ± 1.7	43.6 ± 0.9	44.2 ± 0.1

As reported before[6] and now noted in Figures 5 and 6, the changes of properties at $T > T_g$ are nonmonotonic. A secondary transition at $T_{LL}/T_g = 1.2 \pm 0.1$ has been reported by Boyer,[16] the MCT postulated the crossover transition temperature at $T_c/T_g \approx 1.25 \pm 0.10$ and discussed in theoretical and experimental studies of dynamic structures in molten polymers.[26–29] During cooling there are two MCT relaxations—segmental (at $T > T_c$) and structural (at $T < T_c$). Furthermore, the fast and the elementary relaxations start at temperature in the glassy state and stretch to $T > T_c$. Transitions in glass-forming, fragile liquids at $T > T_g$ repetitively have been reported.[44–49]

In Figure 5 κ versus T dependence of CPNC-17 is shown (see also Figs. 10 and 11 in ref. [6]). Several aspect are worth noting: (1) on this plot the transitions T_g and T_T seem pressure-independent; (2) the transition region, **T**, stretches from about T_g to T_T; (3) the observed in the *PVT* diagrams pressure variation of T_g ranges from $T_g(P = 0)$ to $T_g(P = 190) \approx T_T$.

Figure 6 displays the concentration dependence of α_m at $P = 0$ and its first derivative for PS and its CPNC. Both functions go through a local minimum at $w_{\text{solid}} \approx 3.6$ wt %. Evidently, it is expected that the thermal expansion coefficient should decrease with the solid loading. However, experimentally this takes place only up to the critical clay content of matrix solidification—above this limit further addition of organoclay containing 39 wt % low molecular weight intercalant increases the free volume content and thus the value of α_m.

Glass Transition

The glass transition region is characterized by T_g and $h_g = h_{(T=T_g)}$, both dependent on P and w; T_g increases with P and decreases with w, while

h_g decreases with both P and w. Numerical values of the polynomial fit to T_g and h_g are listed in Table 3. The pressure gradients of T_g and h_g show local extrema at $w_{solid} \approx 3.6$ wt %. On the basis of the free volume argument it is expected that with increasing pressure T_g should increase and h_g should decrease. The pressure gradient of T_g should follow the theoretical prediction of eq 8, but an earlier analysis showed that agreement can be observed only for slow vitrification during isobaric cooling from the melt. By contrast, the "standard" *PVT* procedure resulted in significant differences between the predicted and experimentally found gradients (see Fig. 12 in ref. 6).

Experimental values of dT_g/dP are listed in Table 3. Except data for CPNC-17 all other decrease with P toward zero. The change with the MMT content is complicated, different for each level of P. The absolute magnitude of the gradient, $(dT_g/dP)_{P=0}$ fall within the range reported for amorphous polymers $(dT_g/dP)_{P=0} = 0.29$–0.78 K/MPa and listed for PS by Roe (0.16–0.31).[50] The parameters h_{g0} and b_1 (columns 7 and 8 in Table 3) also show local extrema at $w_{solid} \approx 3.6$ wt %.

Vitrification has been subject of many fundamental studies,[51–54] but many questions remain unanswered. The dynamic studies of relaxations seem to indicate that the vitrification is a net result of temperature and/or pressure engendered reduction of several vibration modes.

The Glassy State

Glass is not a well defined state with regular dynamic behavior. The model made of hard spheres with short range interactions indicated presence of two glassy states; one dominated by repulsions the other by attractions.[55] The presence of two glassy states may justify presence of a glass–glass transition as well as broad distribution of the relaxation times, characteristic for the glass transition α-process.

The model favorably compared with the prediction of the MCT. Polymeric glasses within the range of temperature between T_β and T_g undergoes the "physical aging."[25] The stress relaxation and loss of free volume that accompany the process might lead to changes of shape and dimension of formed article. In particular, the physical aging affects injection molded parts, thus to minimize the aging effects the holding time and pressure as well as 24 h storage before shipping are often used. The aim is reduction of the excess free volume entrapped in the nonequilibrium glass while cooling and pressurizing melt to the ambient conditions. The initial free volume content depends on the cooling rate and the pressure level during vitrification, then during aging time, t_a, h varies as: $h = h(P, T, t_a)$. According to Struik the rate of glass relaxation is most rapid at $T_{max}/T_g = (T_g - T_\beta)/2T_g \approx 0.88 \pm 0.03$, that is, for PS at $T_{max} = 308$–318 K.[25] In the case of CPNC the rate is affected by the presence of clay platelets that form nano-cages, and by the mount of the plasticizing intercalant.

The free volume frozen fraction, FF, calculated from the isobaric temperature dependence of h (see eq 10) is listed in Table 4. As reported earlier, the "standard" *PVT* test method resulted in increase of FF with P; isobaric cooling from $T_g + 30$ yielded nearly constant values, whereas isobaric heating caused a dramatic decrease of FF from 0.69 to 0.50.[6] The effect of the "standard" procedure is easy to understand considering that during the slow pressurization and step-wise heating the specimen undergoes physical aging, thus the free volume slope decreases and FF value increases. The value $FF_0 = 0.64 \pm 0.03$ for PS at $P = 0$ is comparable to an average obtained for several PS resins, viz. $FF_0 = 0.69 \pm 0.01$.[43]

More difficult is explanation of FF >1 values obtained for CPNC with MMT content $w > w_{solid} = 3.6$ wt %. Before the *PVT* test the specimens were heated at 10 MPa to $T \geq 130$ °C and then cooled to 30 °C. However, adsorption and solidification of organic substances on clay surface reduces the free volume by equivalence of T reduction by about 50 °C.[4] Thus, incorporation of an excess of C10A to solidified system brings in a large amount of free volume entrapped within the tightly packed stacks of MMT-2MBHTA. Because of low molecular mobility the free volume at 130 °C is quenched to ~30 °C, that is, to the vicinity of T_β. Then, heating the glass toward T_g increases the rate of physical aging, which translates into reduction of specific and free volume, and thus FF > 1.

The analysis of the *PVT* behavior of CPNC indicates that in these systems there are two kinds of free volume, one associated with the matrix, the other with intercalant. Such a duality has not been observed in well-dispersed nanocomposites at low clay content. In the stud-

ied PS-based CPNC only small portion of clay platelets is exfoliated, most remaining in stacks with the interlayer spacing of similar dimension as in organoclay. Owing to solidification of the matrix polymer its molecular mobility is reduced; at $w_{solid} \approx 3.6$ wt % MMT all PS matrix is physically bonded to clay—incorporation of additional organoclay brings in free volume within the intercalant domains, but this does not affect the matrix.

The physical aging behavior has significant influence on the dimensional stability of molded articles. It involves release of the residual stresses, thus possible warping, as well as a loss of free volume reflected in shrinking. Furthermore, reduction of free volume increases stiffness and brittleness of the moldings. Judging by the PALS results during aging the average free volume cavity size remains constant, but their number decreases.[56,57]

In the absence of direct measurements of physical aging one may only speculate how the presence of clay platelets affects stress relaxation and dimensional stability. There are two aspects: a general one, pertinent within the low clay content (partially exfoliated CPNC) and the other related to the systems with $w > w_{solid}$. For the former case, assuming a two component system (e.g., PA + MMT) the CPNC relaxation is sterically hindered by interacting clay platelets at concentration of critical encompassed volume, that is, ~1.1 wt % clay, thus the physical aging effects should be smaller than these for neat matrix. In the case of highly loaded intercalated systems the situation is more complex since there are two sources of free volume—polymer and intercalant within the excess of organoclay. Since at w_{solid} all PS macromolecules are solidified one may expected that in the vicinity of this composition the rate of physical aging is the lowest. Further incorporation of organoclay with its large amount of low molecular weight intercalant resembles compounding polymer with filler particles and plasticizer—tensile modulus will still increase, but the strength decrease and the rate of physical aging should increase. In conclusion, for highly loaded systems, annealing might be more important compared to neat matrix, and better overall performance are achieved at lower clay loading.

The derivative properties, κ and α coefficients, are shown in Figures 5 and 6, respectively. As expected, the derivatives are more sensitive to changes of structures, but at the same time show greater data scatter than the original *PVT* plot. The coefficients were computed using three moving arch (5-points) procedures and then averaging the results. The *T*-dependence of the compressibility coefficient for the other compositions show are similar to that in Figure 5—exception being the initial negative slope for CPNC with $w > w_{solid}$ at $P > 100$ MPa. The plot of the thermal expansion coefficient, α versus T (see Fig. 6) also shows $\alpha < 1$ for glassy CPNC with high clay content. These effects originate in the decrease of the free volume at increasing T. The thermal expansion coefficient shows significantly greater scatter of data than that of compressibility. Furthermore, its temperature and pressure dependencies are less informative. Thus, α in the melt is almost independent of clay content, whereas its pressure variation in the glassy state is shown in Table 6—it decreased with P; its concentration dependence in the vitreous state goes through a local extremum at w_{solid}.

Table 6. Pressure Coefficients of the Thermal Expansion Coefficient in the Glass, α_g

Sample	α_0	$-100 \times (d\alpha/dP)$	$10^5 \times (d^2\alpha/dP^2)$	r^2
PS	2.63	1.03	1.73	0.989
CPNC-1	2.33	0.97	2.21	0.989
CPNC-2	2.16	1.05	2.81	0.997
CPNC-5	0.966	1.16	3.83	0.995
CPNC-10	0.321	1.49	6.48	0.941
CPNC-17	0.213	1.35	5.43	0.917

In Figures 5 and 6 the secondary transition at $T_T \approx 1.2T_g$ are indicated by a vertical straight line; in Figure 5 the glass transition at ambient pressure is also marked by vertical line—the line forms a boundary between the vitreous and transitory regions. It is noteworthy that in both Figures the T_g determined by *PVT* and DSC (see part 4.2) is marked by solid line with negative slope that intersects the transitory region. Comparing Figure 5 with Figure 1 makes it evident that in both the vertical line from T_g at $P = 0.1$ MPa provides a boundary between the glass and **T**-region. However, at the same time in Figure 1 the transition marked as T_T is invisible, and so is T_g in Figure 5.

One might ponder the origin/mechanism of the pressure-independent phenomena marked by the vertical lines in Figures 1, 5, and 6. Since increase of P reduces the free volume and in

turn restricts segmental motion the left vertical line does not mark T_g even when it starts at $T_{g,\ P=0}$. However, while the glass transition is related to the viscosity controlling α-process observed in any glass-former, in polymers another dynamic process starts near T_g—it is the E-process, elementary for macromolecules.[52] It involves local conformational transitions of the backbone chain on a picoseconds scale with low potential energy barrier, thus insensitive to T and P.[58] Validity of the latter statement might be questioned as the experimental and simulation studies are carried out for a range of T, but at atmospheric P.

The second vertical line starts at T_T, might be associated with Boyer T_{LL}, with Ngai's T_B or with T_c of the MCT. The former, $T_{LL}/T_g = 1.2 \pm 0.1$, is pressure sensitive: $[dT_{LL}/dP_{PS} = 0.6$ (K/MPa)],[20] and as such cannot explain the observed behavior. Ngai's transition at $T_B/T_g = 1.2$–1.7 is defined by two intersecting lines representing the Vogel-Fulcher-Tammann-Hesse (VFTH) expression:

$$\tau(T) = \tau_0 \exp\{B/(T - T_0)\} \qquad (14)$$

where τ is the segmental relaxation time, while τ_0 and B being equation constants.[29] However, since VFTH relation is based on free volume it is highly probable that isobaric experiments at different level of P will lead to different value of T_B. The equations of state indicate equivalence of P with some function of T, for example, see eq 2 for constant value of V and h. If so, than MCT should also lead to crossover pressure, P_c, equivalent to T_c.[59]

Mathematically, the crossover temperature, T_c, comes from the MCT expression for the relaxation time:[60]

$$\tau \propto (T - T_c)^{-\gamma} \qquad (15)$$

where γ is a universal exponent. The relation predicts that as T approaches T_c the $\tau \to \infty$. In other words, the model system vitrifies at T_c, even while experimentally vitrification is observed not at T_g but at $T_c \approx 1.2T_g$. However, the liquid-like behavior is predicted and observed at $T > T_c$. This may help in explaining the existence of T_T, but it does not lead to any conclusion regarding its pressure insensitivity. Some years ago the photon correlation spectroscopy was applied for study of relaxations in acrylic polymers at $T > T_g$.[61] The authors modified eq 14 by setting $B = aP$, where a is a numerical parameter. The empirical relation resulted in "master curve" dependence within the full range of T and P implying pressure independence for T_0. However, if the master curve behavior of molten polymer extends to the MCT divergence of eq 15, then its P-independence might be expected.

Unfortunately, there are few theoretical or experimental data to shed light on the problem of the two pressure-independent limits observed for the two *PVT* derivatives in Figures. 5 and 6. Nevertheless, the two isobaric limiting temperatures are real, observed for neat PS resins studied in three laboratories as well as for the PS-based CPNC specimens in full range of compositions.

SUMMARY AND CONCLUSIONS

PS was melt compounded with Cloisite-10A (C10A; $w = 0$–17.1 wt % MMT). The *PVT* behavior of these molten and glassy systems was examined using the Simha-Somcynsky equation-of-state (eos). In the molten state the theoretical description provided excellent fit to the *PVT* surface with $\pm$ 0.0003 mL/g residuals of the specific volume, yielding the characteristic reducing parameters, P^*, V^*, T^*, and the free volume parameter, $h = h(V, T)$. On the basis of XRD and HRTEM studied the system was modeled as intercalated stacks with solidified layer of the matrix polymer dispersed in "free" PS melt. The model also predicted that the free PS should disappear at $w_{solid} \approx 3.6$ wt % MMT—above this limit C10A remains largely unaffected by compounding. From the P^*, V^*, T^* parameters the Lennard-Jones (L-J) bulk-average interaction quantities, $\langle \varepsilon^* \rangle$ and $\langle v^* \rangle$ were computed, and then the binary interaction parameters, ε^*_{ij} and v^*_{ij}, were calculated for polymer (11), for stacks (22), and for stack-polymer (12).

On the *PVT* surface the glass transition region is characterized by T_g, and associated with it the free volume function $h_g = h(T_g)$, both depended on P and w. It was found that T_g increases with P and decreases with w, whereas h_g decreases with P and w. The pressure gradients of these functions showed local extrema at $w = w_{solid}$. In the vitreous region the V versus T and h versus T slopes depend on w; for PS the slopes are positive, decreasing with clay content toward negative values. The defined in terms of these slopes free volume frozen fraction, FF, ranges from FF ≈ 0.6 for PS to 1.6 for CPNC-17 at 160 MPa. The ambient pressure value of FF and its first derivative of P

show local extrema at the concentration of free PS disappearance, $w_{solid} = 3.6$ wt %.

In addition to the fundamental analysis of the *PVT* data by means of S-S eos, the derivatives: the thermal expansion coefficient, $\alpha = \alpha(T, P, w)$, and the compressibility coefficient, $\kappa = \kappa(T, P, w)$, were computed. The former decreased with P; its concentration dependence in the molten state was slight, but in the vitreous state it changed with w going through a local extremum at w_{solid}. The κ versus T dependence revealed two secondary transitions, one below and second above T_g; $T_T/T_g = 1.2 \pm 0.1$. The two transitions appeared to be P-independent.

This and several other articles in this issue are dedicated to Professor Robert Simha. Unfortunately, the initial idea of celebrating his 95th birthday has been transformed by his passing on into a memorial issue. Robert was excellent teacher, a model scientist but foremost good, personal friend for nearly five decades. His numerous and fruitful discussions, the guidance and vivid interest in the evolution of the text left his stamp on the manuscript.

NOMENCLATURE

Abbreviations

CPNC	Clay-containing polymeric nanocomposites
DSC	Differential scanning calorimetry
eos	Equation-of-state
FF	Frozen in free volume fraction
HCP	Hairy clay platelets
HRTEM	High resolution transmission electron microscopy
L-J	Lennard-Jones
MCT	Mode-coupling theory
MMT	Montmorillonite
MW	Molecular weight
NMR	Nuclear magnetic resonance
PA	Polyamide
PLA	Polylactic acid
PNC	Polymeric nanocomposites
PS	Polystyrene
PVT	Pressure-volume-temperature dependence
SEM	Scanning electron microscopy
S-S	Simha-Somcynsky cell-hole theory or eos
T	Transition zone
VFTH	Vogel-Fulcher-Tammann-Hesse relation or temperature
XRD	X-ray diffraction

Symbols

$\tilde{F}$	Helmholtz free energy in reduced variables
$3c$	The external, volume-dependent degrees of freedom per macromolecule
CD	Coefficient of determination
d_{001}	Interlayer spacing
FF	Isothermal frozen free volume fraction
h	Free volume parameter in S-S eos; $h = h(V, T)$
h_g	h-value at T_g
m	Number of clay platelets per stack
M_s	M_n/s molecular weight of statistical segment
M_n, M_w	number- and weight-average molecular weight
P, P^*	Pressure and the characteristic pressure reducing parameter
P^0	The glass formation pressure
q	Rate of vitrification by either cooling or compressing
R	The gas constant
r^2	Correlation coefficient squared
s	Number of statistical segments per macromolecule
T, T^*	Temperature and the characteristic temperature reducing parameter
T_B	Ngai's secondary transition temperature
t_a	Annealing time
T_c	Crossover transition temperature, $T_c/T_g = 1.25 \pm 0.10$
T_g	Glass transition temperature
T_{LL}	Liquid–liquid transition temperature, $T_{LL}/T_g = 1.2 \pm 0.1$
T_m	Melting point
T_{max}	Temperature at which the physical aging rate is the highest
T^0	The glass formation temperature
T_β	Beta subglass transition temperature
v^*	L-J segmental repulsion volume per statistical segment
V, V^*	Specific volume and the characteristic volume reducing parameter
w, w_{solid}	Clay content and its value for full solidification of the matrix
x_i	Mole fraction
X_i	Site fraction
y	Occupied volume fraction in S-S eos; $h = 1-y$
z	Coordination number
zq	The number of interchain contacts in a lattice; $zq = s(z-2) + 2$
ϕ	Cluster concentration
ε^*	L-J maximum attractive energy
Δ	Difference between values for the liquid (l) and glassy state (g)
α	Thermal expansion coefficient
η	Viscosity
κ	Compressibility
σ	Standard deviation
	Independent variables in the glassy state are indicated by "prime," viz. T', and P'
	Tilde indicates reduced variables, for example, as defined in eq 4.

DOI 10.1002/polb

REFERENCES AND NOTES

1. Utracki, L. A. Clay-Containing Polymeric Nanocomposites, Vol. 2: Monograph; RAPRA: Shawbury, Shropshire, UK, 2004.
2. Ray, S. S.; Okamoto, M. Prog Polym Sci 2003, 28, 1539–1641.
3. Simha, R.; Utracki, L. A.; Garcia-Rejon A. Compos Interfaces 2001, 8, 345–353.
4. Utracki, L. A.; Simha, R.; Garcia-Rejon A. Macromolecules 2003, 36, 2114–2121.
5. Utracki, L. A.; Simha, R. Macromolecules 2004, 37, 10123–10133.
6. Utracki. L. A. J Polym Sci Part B: Polym Phys 2007, 45, 270–285.
7. Simha, R.; Somcynsky, T. Macromolecules 1969, 2, 342–350.
8. Somcynsky, T.; Simha, R. J Appl Phys 1971, 42, 4545–4548.
9. (a) Prigogine, I.; Bellemans, A.; Naar-Colin, C. J Chem Phys 1957, 26, 710; (b) Prigogine, I.; Bellemans, A.; Naar-Colin, C. J Chem Phys 1957, 26, 751–755.
10. Jain, R. K.; Simha, R. Macromolecules 1980, 13, 1501–1508.
11. Jain, R. K.; Simha, R. Macromolecules 1984, 17, 2663–2668.
12. Simha, R.; Jain, R. K.; Jain, S. C. Polym Compos 1984, 5, 3–10.
13. Papazoglou, E.; Simha, R.; Maurer, F. H. J Rheol Acta 1989, 28, 302–308.
14. Utracki, L. A.; Lyngaae-Jørgensen, J. Rheol Acta 2002, 41, 394–407.
15. Hentschke, R. Macromol Theory Simul 1997, 6, 287–316.
16. Israelachvili, J. N.; Tirrell, M.; Klein, J.; Almog, Y. Macromolecules 1984, 17, 204–209.
17. Horn, R. G.; Israelachvili, J. N. Macromolecules 1988, 21, 2836–2841.
18. Luengo, G.; Schmitt, F.-J.; Hill, R; Israelachvili, J. N. Macromolecules 1997, 30, 2482–2494.
19. Boyer, R. F. In Encyclopedia of Polymer Science and Technology, Suppl. Vol. 2; Mark, H. F., Ed.; Wiley: New York, 1977; pp 745–839.
20. Boyer, R. F. J Macromol Sci Phys 1980, 18, 461–553.
21. Boyer, R. F. In Order in the Amorphous State, Miller, R. L.; Rieke J. K., Eds.; Plenum: New York, 1987.
22. Cowie, J. M. G.; McEwen, I. J.; McIntyre, R. In Polymer Blends Handbook; Utracki L. A., Ed.; Kluwer Academic Press: Dordrecht, 2002.
23. Quach, A.; Simha, R. J Appl Phys 1971, 42, 4592–4606.
24. Quach, A.; Simha, R. J. J Phys Chem 1972, 76, 416–421.
25. Struik, L. C. E. Physical Aging in Amorphous Polymers and Other Materials; Elsevier: Amsterdam, 1978.
26. Kisliuk, A.; Mathers, R. T.; Sokolov, A. P. J Polym Sci B: Polym Phys 2000, 38, 2785–2790.
27. Casalini, R.; Roland, C. M. Phys Rev B 2005, 71, 014210.
28. Ngai, K. L. J Non-Cryst Solids 2000, 275, 7–51.
29. Ngai, K. L. J Phys Condens Matter 2003, 15, S1107–S1125.
30. McKinney, J. E.; Simha, R. Macromolecules 1974, 7, 894–901.
31. McKinney, J. E.; Simha, R. Macromolecules 1976, 9, 430–441.
32. McKinney, J. E.; Simha, R. J Res Natl Bur Stand Sect A: Phys Chem 1977, 81, 283–297.
33. Curro, J. G.; Lagasse, R. R.; Simha, R. J Appl Phys 1981, 52, 5892–5897.
34. Tanoue, S.; Utracki, L. A.; Garcia-Rejon, A.; Tatibouët, J.; Cole, K. C.; Kamal, M. R. Polym Eng Sci 2004, 44, 1046–1060.
35. Tanoue, S.; Utracki, L. A.; Garcia-Rejon, A.; Sammut, P.; Ton-That, M.-T.; Pesneau, I.; Kamal, M. R.; Lyngaae-Jørgensen, J. Polym Eng Sci 2004, 44, 1061–1076.
36. Tanoue, S.; Utracki, L. A.; Garcia-Rejon, A.; Tatibouët, J.; Kamal, M. R. Polym Eng Sci 2005, 45, 827–837.
37. Zoller, P.; Walsh, D. Standard Pressure-Volume-Temperature Data for Polymers; Technomic Pub. Co.: Lancaster-Basel, 1995.
38. Simha, R.; Wilson, P. S.; Olabisi, O. Kolloid-Z u Z Polym 1973, 251, 402–408.
39. Utracki, L. A.; Simha R. Macromol Chem Phys Molecul Theory Simul 2001, 10, 17–24.
40. Kovacs, A. J. J Polym Sci 1958, 30, 131–147.
41. Kovacs, A. J.; Hutchinson, J. M. J Polym Sci Polym Phys Ed 1979, 17, 2031–2058.
42. Eisenberg, A.; Shen, M. C. Rubber Chem Technol 1970, 43, 156–170.
43. Utracki, L. A. Polymer 2005, 46, 11548–11556.
44. Murthy, S. S. N. J Mol Liq 1990, 44, 211–230.
45. Murthy, S. S. N. J Polym Sci Part B: Polym Phys 1993, 31, 475–480.
46. Murthy, S. S. N.; Kumar, D. J. Chem Soc Faraday Trans 1993, 14, 2423–2427.
47. Angell, C. A. In Relaxation in Complex Systems; Ngai, K. L.; Wright G. B., Eds.; NRL: Washington DC, 1985.
48. Angell, C. A. Science 1995, 267, 1924–1935.
49. Böhmer, R.; Ngai, K. L.; Angell, C.; Plazek, D. J Chem Phys 1993, 99, 4201–4209.
50. Roe, R.-J. In Encyclopedia of Polymer Science and Technology, 2nd ed.; Mark H. F., Ed., Wiley: New York, 1987; Vol. 7, pp 531–544.
51. Jäckle, J. Rep Prog Phys 1986, 49, 171–231.
52. Kanaya, T.; Kaji, K. Adv Polym Sci 2001, 154, 87–141.
53. Binder, K.; Baschnagel, J.; Paul, W. Prog Polym Sci 2003, 28, 115–172.
54. Bicerano, J. In Encyclopedia of Polymer Science and Technology, 3rd ed, Mark, H. F., Ed., Wiley: Hoboken, NJ, 2003.

55. Pham, K. G.; Puertas, A. M.; Bergenholtz, J.; Egelhaaf, S. U.; Mousaid, A.; Pusey, P. N.; Schofield, A. B.; Cates, M. E.; Fuchs, M.; Poon, W. C. K. Science 2002, 296, 104–106.
56. Cangialosi, D.; Schut, H.; van Veen, A.; Picken, S. J. Macromolecules 2003, 36, 142–147.
57. Cangialosi, D.; Wübbenhorst, M.; Schut, H.; Picken, S. J Acta Phys Polonica A 2005, 107, 690–696.
58. Okada, O.; Furuya, H.; Kanaya, T. Polymer 2002, 43, 977–982.
59. Baschnagel, J.; Varnik, F. J Phys Condens Matter 2005, 17, R851–R953.
60. Reichman, D. R.; Charbonneau, P. J. Statistical Mech: Theory Experim 2005, P05013.
61. Fytas, G.; Meier, G.; Patkowski, A.; Dorfmüller, Th. Colloid Polym Sci 1982, 260, 949–955.